Chinese Journal of
POLYMER SCIENCE

RESEARCH ARTICLE

https://doi.org/10.1007/s10118-024-3097-5
Chinese J. Polym. Sci. **2024**, *42*, 798–804

Effect of Phase Separation Size on the Properties of Self-healing Elastomer

Jun Xu[a,†], Lei Zhu[a,†], Xian-Qi Feng[b], Cong Sui[a], Wen-Peng Zhao[a,c*], and Shou-Ke Yan[c,d*]

[a] *School of Chemical Engineering, Qingdao University of Science & Technology, Qingdao 266042, China*
[b] *College of Engineering, Yanching institute of Technology, Langfang 065210, China*
[c] *Key Laboratory of Rubber-plastics, Qingdao University of Science & Technology, Qingdao 266042, China*
[d] *State Key Laboratory of Chemical Resource Engineering, Beijing University of Chemical Technology, Beijing 100029, China*

Electronic Supplementary Information

Abstract Regulation of phase structure has been recognized as one of the most effective ways to fabricate self-healing polymers with high mechanical strength. The mechanical properties of the resultant polymers are certainly affected by the size of separated phase domain. However, the study on this aspect is absence, because it can hardly exclude the influence of variation in monomer proportion required for tuning the separated phase size. Here, we report the first study on tuning the phase size through reversible addition-fragmentation chain transfer (RAFT) polymerization without changing the proportion of monomers. As expected, the size of separated phase has been successfully mediated from 15 nm to 9 nm by tuning the molecular weight of the chain transfer agent. It is found that the mechanical strength and the self-healing efficiency of the resultant polymers increase simultaneously with the decrease of phase size. The study on the formation kinetics of hydrogen bonds reveals that the decrease of phase size can facilitate the re-bonding rate of hydrogen bonds, even if the migration of polymer chains is restricted.

Keywords Self-healing polymers; Phase separation; Reversible addition-fragmentation chain transfer

Citation: Xu, J.; Zhu, L.; Feng, X. Q.; Sui, C.; Zhao, W. P.; Yan, S. K. Effect of phase separation size on the properties of self-healing elastomer. *Chinese J. Polym. Sci.* **2024**, *42*, 798–804.

INTRODUCTION

Imparting polymer materials with self-healing ability can certainly extend their service life and enhance their reliability in practical applications, which are beneficial to realize a sustainable society.[1–7] The intrinsic self-healing polymers have been attracted wide interesting of researchers due to their repeatable self-healing ability.[8–10] For this kind of polymers, high mechanical properties are, however, generally achieved at the expense of their self-healing ability, which severely restricts their applications.[11–13] To address this conflict, enormous endeavors have been dedicated for designing self-healing polymers with high mechanical strength and superior self-healing ability by constructing particular micro- or nano-structures, such as hydrogen-bonding array,[14] bionic structures,[15,16] phase separation structures,[17–20] and so forth. Among them, phase separation structure induced by hard/soft or/and hydrophilic/hydrophobic segments, as well as supramolecular self-assembly has been proved to be an effective method for direct fabricating robust self-healing polymers.[21,22]

It has been reported that the separated phase structures in the polymers serve as nanofillers to improve their mechanical strength.[23] In this case, the phase structure and size of separated phase domains, *i.e.*, the phase size, exhibits certainly effect on the mechanical properties of the resultant polymers. The effect of phase size on the mechanical properties has, however, rarely been studied, because it can hardly exclude the influence of monomer variation for purposeful tuning the phase size. For example, the phase structure of self-healing polymers caused by separation of hard and soft segments is generally fabricated through polycondensation of the related hard and soft segments.[24] Consequently, the regulation of phase size can only be realized by changing either the sort of monomer or the monomer proportion, which show also evident influence on the mechanical properties of the resultant polymer. On this account, tuning the domain size of separated phase without changing the proportion of monomers is prerequisite to investigate the influence of phase size on the mechanical properties of self-healing polymers.

Self-healing polymers based on hydrogen bonding exhibit many excellent characteristics, such as fast self-healing speed, mild self-healing condition, adjustable mechanical properties and so forth, and thus have attracted intensive interest.[25] Recently, Sun *et al.*[23] constructed a self-healing polymer composite of hydrophilic poly(acrylic acid) (PAA) and

* Corresponding authors, E-mail: zhwp@qust.edu.cn (W.P.Z.)
E-mail: skyan@mail.buct.edu.cn (S.K.Y.)
† These authors contributed equally to this work.
Received December 6, 2023; Accepted January 16, 2024; Published online March 7, 2024

polyvinylpyrrolidone (PVP) based on hydrogen bonding. The phase structures were formed through the hydrophobic interaction between the pyrrolidone groups. The regulation of phase size is, however, also realized by tuning the proportion of PAA and PVP. In our previous studies,[26–30] we fabricated fast self-healing polymers (defined as PA) based on hydrogen bonding through free radical polymerization of poly(ethylene glycol) 480 methyl ether acrylate (MPEG480) and acryloylmorpholine (ACMO). It should be pointed that the morpholine group in ACMO exhibits actually a similar structure as pyrrolidone in PVP. Therefore, we infer that separated phase structures may also be generated through the hydrophobic interactions among morpholine groups. In this case, the phase size of it can be regulated simply by tuning the chain length of it. To check this, reversible addition-fragmentation chain transfer (RAFT) polymerization has been used to regulate the chain structure of the polymer and its phase separation structure has been studied. As expected, the phase size can be successfully mediated from 15 nm to 9 nm by tuning the molecular weight of chain transfer agent (CTA) without changing the sort of monomer or the monomer composition. The glass transition temperature (T_g) increases from 28.1 °C to 47.5 °C with the decline of phase size from 15 nm to 9 nm. As a result, the mechanical strength of the elastomer exhibits uptrend with the decrease of phase size. Interestingly, the decline of phase size can facilitate the exchange rate of hydrogen bonding within the elastomer. Therefore, the self-healing ability of the elastomers increases, even if their strength and T_gs are improved.

EXPERIMENTAL

Materials

Carbon disulfide, chloroform, acetone, toluene, tetrabutylammonium bisulfate, NaOH, and HCl were purchased from Yantai Sanhe Chemical Reagent Co., LTD. Poly(ethylene glycol) methyl ether acrylate (MPEG, 99 %, Aladdin, China), Acryloylmorpholine (ACMO, 98%, Aladdin, China), potassium persulfate (KPS, initiator, 99.5%, Bodi, China), *N*,*N*,*N*′,*N*′-tetramethylethyl enediamine (TEMED, 99.5%, Aladdin, China), were all used without further purification. Distilled water was used for all experiments.

Synthesis of CTA

A certain amount of carbon disulfide (0.36 mol), chloroform (0.9 mol), acetone (0.9 mol), and tetrabutylammonium hydrogen sulfate (7.1 mmol) were mixed with 120 mL of petroleum ether in a 1 L boiling flask-4-neck cooled with ice bath under nitrogen atmosphere. NaOH solution with a mass fraction of 50% was then added dropwise into the solution. 900 mL of water was added to dissolve the reaction products after stirring for 8 h. Concentrated HCl (120 mL) was thereafter added slowly to acidify the aqueous layer, and stirred for 30 min under N_2 purge. The product was obtained after filtering and washing thoroughly with deionized water. After drying at 60 °C in an oven, the resultant powder was washed with a mixture of toluene/acetone with a volume ratio of 4/1, and finally obtained a light-yellow powder.

Synthesis of Macro-CTA

Different amounts of ACMO (0.5668 g, 0.2834 g, 0.1889 g), CTA (0.002mmol) and 10 mL of deionized water were added to a 50 mL flask stirring for 30 min under nitrogen atmosphere. After the solution was heated to 40 °C, KPS (0.2 mL, 2 wt% aqueous solution) and TEMED (0.2mL) were added and reacted for 3 h, yielding the macro-CTA.

Synthesis of RPA-*n*

Taking RPA-4 as an example: after macro-CTA-4 was cooled to room temperature MPEG (1.944 g) and ACMO (1.7004 g) were added and stirred for 30 min under nitrogen atmosphere. The solution was then cooled down to 0 °C using ice bath and vacuum degassing for another 30 min before KPS (0.2 mL) and TEMED (0.2 mL) were added. The mixture was finally transferred to tailored glass tubes and polymerized at desired temperature for 12 h to obtain the precursor hydrogel. The precursor hydrogels were first washed thoroughly with distilled water to remove the unreacted monomers. The elastomers were obtained by air-drying the precursor hydrogels for 12 h and followed by drying for another 12 h at 60 °C.

Characterization

The mechanical properties were characterized using a UTM2502 electronic universal testing machine (SUNS, China) at room temperature in air (at 20%–40% humidity) with a tensile speed of 50 mm/min. The self-healing measurement was as below: the rod-like sample was cut thoroughly using a blade and the fresh fracture surfaces were then put together gently. The reunite sample was allowed to heal at room temperature for 10 s. The healing efficiency of the sample was calculated from the ratio of the ultimate tensile strength before and after healing. The temperature-dependent FTIR spectra were recorded *in situ* in the range of 4000–400 cm^{-1} with 16 scans at a resolution of 4 cm^{-1} using a Vertex 70 spectrometer (Bruker, GER) equipped with a hot stage (Linkam, UK). The glass transition temperature was determined using dynamic mechanical analysis (DMA, TAQ800) in tension mode under a frequency of 10 Hz, with a heating rate of 5 °C/min in the temperature range from −60 °C to 80 °C. TEM observation was performed on a HT-7800 microscope with an accelerated voltage of 200 kV. Before TEM observation, the ultrathin sections of RPA-*n* were stained by dropping the solution of phosphotungstic acid (1 wt%) onto a copper mesh. After 60 s, the excess phosphotungstic acid solution on the copper grid was gently wiped with filter paper and dried at room temperature. NMR spectra were recorded on a Bruker AVANCE NEO 400 MHz NMR spectrometer (^{1}H-NMR 400 MHz) at 298 K. GPC experiments were performed on an Agilent HPLC system equipped with a model 1260 Hip degasser, a model 1260 Iso pump and a model 1260 differential refractometer detector with using THF as mobile phase at a flow rate of 1.0 mL·min^{-1} at 40 °C. One PLgel 5 μm guard column and three Mz-Gel SDplus columns (10^3 Å, 10^4 Å and 10^5 Å, linear range of M_w=1000–2×10^6 Da) were connected in series. The molecular weight and dispersity were calculated using polystyrene as standard. The sample concentration used for GPC analyses was 5–10 mg·mL^{-1}.

RESULTS AND DISCUSSION

As illustrated in Fig. 1(a), the synthesis of the target polymer can be divided into three steps. (i) The trithiocarbonate with two homolytic leaving groups named as *S*-ethyl-*S*′-(*α*,*α*′-dimethyl-*α*″-acetic acid) trithiocarbonate (EMP), synthesized *via* a one-pot procedure reported by Lai *et al*.,[30] was used as CTA. Its struc-

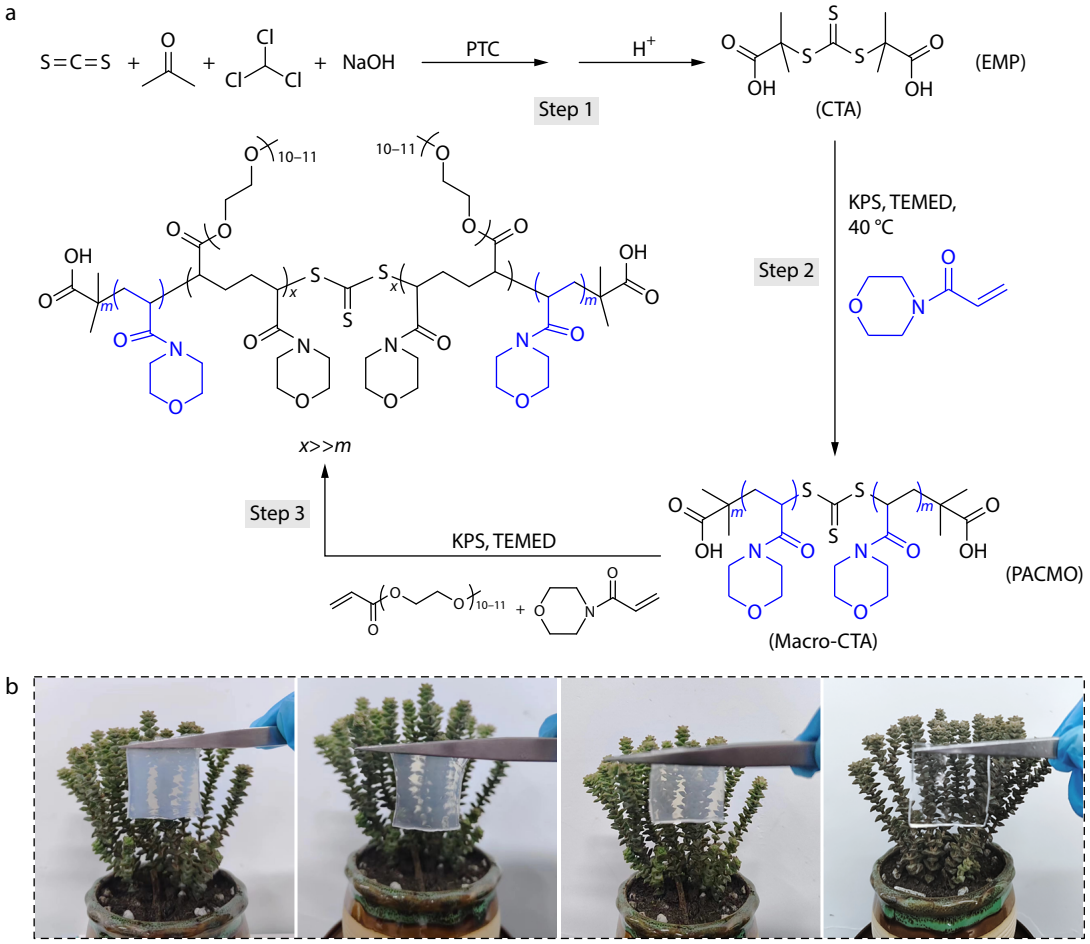

Fig. 1 (a) The synthetic procedure of the self-healing polymer by RAFT polymerization; (b) The real photos of the RPA-4, RPA-8 and RPA-12 precursor hydrogels (from left to right) and the one of free radical polymerization of ACMO and MPEG with the same monomer mass ratio and concentration as RPA-*n* samples denoted as PA (rightmost).

ture has been confirmed by the corresponding ^{1}H-NMR spectrum shown in Fig. S1 (in the electronic supplementary information, ESI). (ii) The CTA obtained in (i) was reacted with certain amount of acryloylmorpholine (ACMO) to produce macro-CTA, and the chain structure of target polymer has been regulated through changing the molecular weight of macro-CTA by tuning the weight of ACMO. The macro-CTAs were named as macro-CTA-4, macro-CTA-8 and macro-CTA-12 for the weight ratio of total ACMO and ACMO used in (ii) *i.e.*, 4, 8 and 12, respectively. Tetrahydrofuran (THF) gel permeation chromatography (GPC) studies indicate that the molecular weight of macro-CTAs increase from M_n=1.81×10^4 g·mol^{-1} for macro-CTA-12 to M_n=4.62×10^4 g·mol^{-1} for macro-CTA-4 with the increasing amount of ACMO (see in Fig. S2 in ESI). Taking macro-CTA-4 as an example, the structure of it was evidently confirmed by the ^{1}H-NMR spectrum shown in Fig. S3 (in ESI). (iii) The resultant macro-CTA-*n* (*n*=4, 8, 12) were reacted with ACMO and poly(ethylene glycol) 480 methyl ether acrylate (MPEG) to fabricate the desired polymers with tunable phase separation structure, named as RPA-*n*.

The left three images shown in Fig. 1(b) are the real photos of precursor hydrogels of RPA-4, RPA-8 and RPA-12 (from left to right), respectively, while the rightmost one exhibits the precursor hydrogel obtained through free radical polymerization of ACMO and MPEG with the same monomer mass ratio and concentration as RPA-*n* samples, denoted as PA. It is obvious that the PA precursor hydrogel is completely transparent, indicating that it possesses a homogeneous network structure. In contrast, the precursor hydrogels of RPA-*n* exhibit a downward trend in transparency, manifesting the occurrence of phase separation. Moreover, the transparency of the precursor hydrogels decreases with the increase of macro-CTA molecular weight, indicating that the phase separation structure can be regulated by tuning the molecular weight of macro-CTA. The phase separation originates from the hydrophobic interactions between morpholine groups in ACMO, like the pyrrolidone groups in PVP.[23]

As illustrated in Fig. 2(a), the RPA-*n* polymer chains contain two segments, *i.e.*, the random P(ACMO-*co*-MPEG) (red) and PACMO (blue) segments. The hydrophobic interactions among morpholine groups in ACMO compels the blue segments together to form the separated phase structures. To verify the phase separation structure, transmission electron microscopy (TEM) characterization was carried out. The RPA-*n* samples were first sliced into ultrathin films, and then stained with sodium phosphotungstate. Figs. 2(b)–2(d) show the phase contrast bright field TEM images of RPA-4, RPA-8 and RPA-12, respectively. The hydrophobic assembled PACMO

https://doi.org/10.1007/s10118-024-3097-5

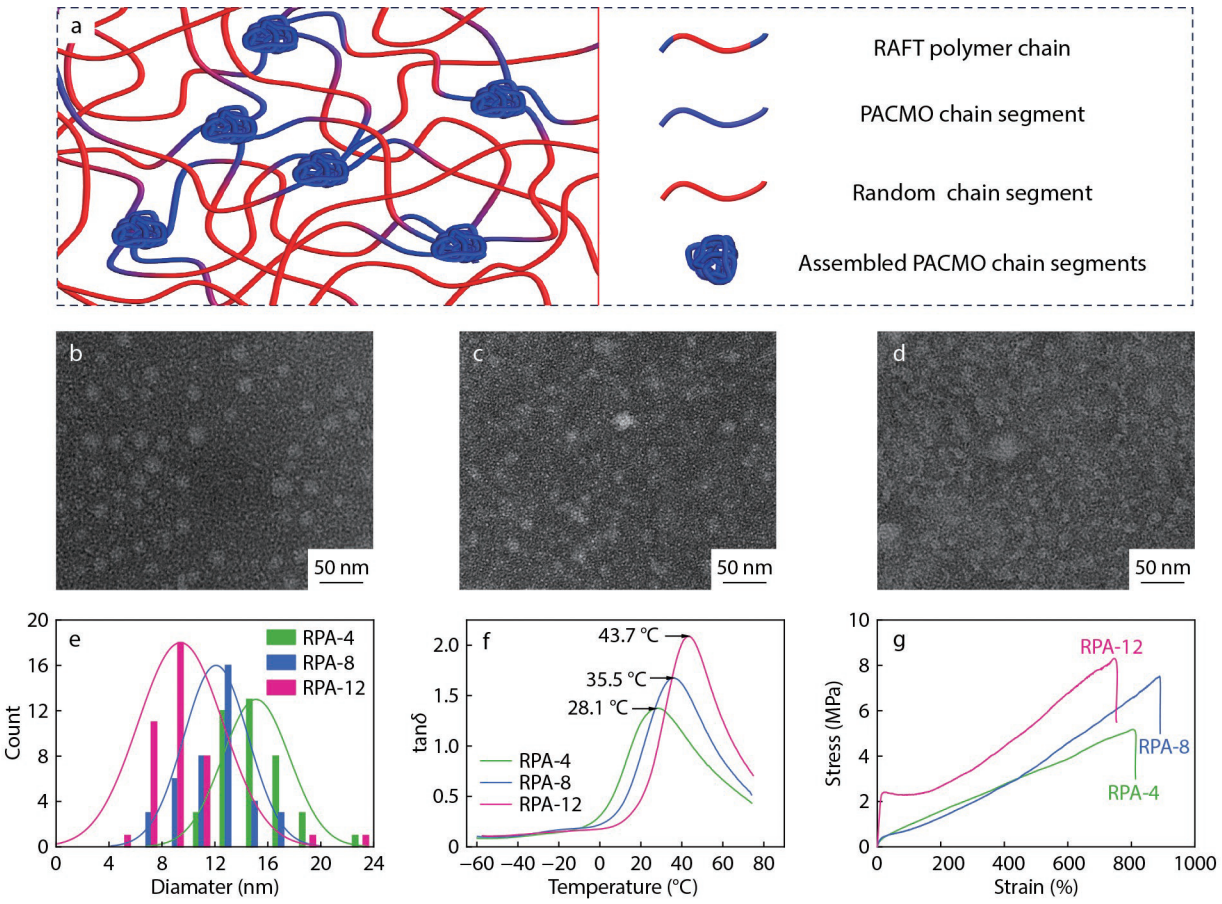

Fig. 2 (a) Sketch of phase structure for RPA-*n* polymers; TEM images of RPA-4 (b), RPA-8 (c), RPA-12 (d), respectively, and their corresponding phase size distributions (e); The damping coefficient *i.e.*, tanδ, curves (f) and stress-strain curves (g) of the resultant polymers.

domains cannot be strained by sodium phosphotungstate and thus exhibit bright contrast in phase contrast TEM images, which uniformly disperse in the RPA-*n* matrix. In sharp contrast, the TEM image of PA fabricated by free radical polymerization displays a homogenous structure (shown in Fig. S4 in ESI), which confirms that the phase separation in RPA-n originates from PACMO segments. Fig. 2(e) shows the phase size distribution of RPA-*n* calculated from Figs. 2(b)–2(d). It is clear that the mean size of the separated phase domains (MSPD) increases with the increasement of used ACMO amount in (ii). In another words, the MSPD of RPA-*n* has been successfully mediated from 9 nm to 15 nm by simple tuning the molecular weight of macro-CTA from 1.81×10^4 g·mol^{-1} to 4.64×10^4 g·mol^{-1} without changing the proportion and total concentration of monomers, which is a prerequisite to reveal the influence of phase size on the properties of self-healing polymers.

The effect of MSPD on T_g of polymer was first investigated through dynamic mechanical analysis. As shown in Fig. 2(f), the MSPD affects T_g of the resultant polymers significantly. The T_gs of RPA-*n* are 28.1 °C for RPA-4, 35.5 °C for RPA-8 and 43.7 °C for RPA-12 with the MSPD of 15, 12 and 9 nm, respectively. The variation of T_gs certainly affects the molecular chain segment mobility of the polymer and thus influences definitely the mechanical properties of RPA-*n*. To quantitatively analyze the effect of phase size on the mechanical properties of the resultant polymers, static tensile tests of RPA-*n* were carried out. Fig. 2(g) displays the stress-strain curves of RPA-*n* samples. From Fig. 2(g), two things should be addressed here. First, it is obvious that the ultimate mechanical strengths of the samples increase from 5.2 MPa to 7.5 MPa and then 8.4 MPa with the MSPD decreases from 15 nm to 12 nm and then 9 nm. Meanwhile, the values of elastic modulus and toughness exhibit the same varying tendency with mechanical strength (see in Fig. S5 in ESI). It should be noticed that the elastic modulus of RPA-4 is similar to that of RPA-8, which is about one-fourth of that for RPA-12. Second, compared with the mechanical properties of PA sample (with a tensile stress/strain of 4.4 MPa/640%, see in Fig. S6 in ESI), the incorporation of phase structure enhances the stress and strain of RPA-n simultaneously. These results clearly reflect that (i) the phase separation structure can definitely improve the mechanical strength of polymers, and (ii) the mechanical properties of the resultant polymers increase with decrease of phase size. Unfortunately, we cannot fabricate the elastomer with MSPD smaller than 9 nm. It is thus difficult to say what will happen if the MSPD further decreases to few nanometers or even to sub-nanometer. According to Pan *et al.*,[31] nanoscale phase mainly dominates the tensile behavior of polymer, while sub-nanoscale phase mainly governs the viscoelasticity. Based on this, we predict that (i) the mechanical strength of the elastomers would increase with the decline in

the MSPD within nanoscale, and (ii) further decrease MSPD to sub-nanometer may decrease the tensile strength of the elastomer in some extent.

To investigate the effect of MSPD on the self-healing ability of the RPA-*n*, the samples were cut into two pieces and the fresh cutting interfaces were then brought together gently to heal. The stress-strain curves of the healed RPA-*n* are shown in Figs. 3(a)–3(c). It can be seen that, only healing for 10 s, the healed samples achieve a tensile strength of 4.8 MPa for RPA-4, 6.9 MPa for RPA-8 and 7.8 MPa for RPA-12 with a healing efficiency of 89%, 91.6% and 92.7% (see in Fig. S7 in ESI), respectively. It is obvious that the mechanical strength and healing efficiency, two important properties that normally trade-off with each other, increase simultaneously with the decrease of phase size, indicating that the conflict between strength and healing efficiency in self-healing polymers can be dispelled by tuning the size of separated phase. Moreover, the resultant elastomers exhibit much faster healing speeds

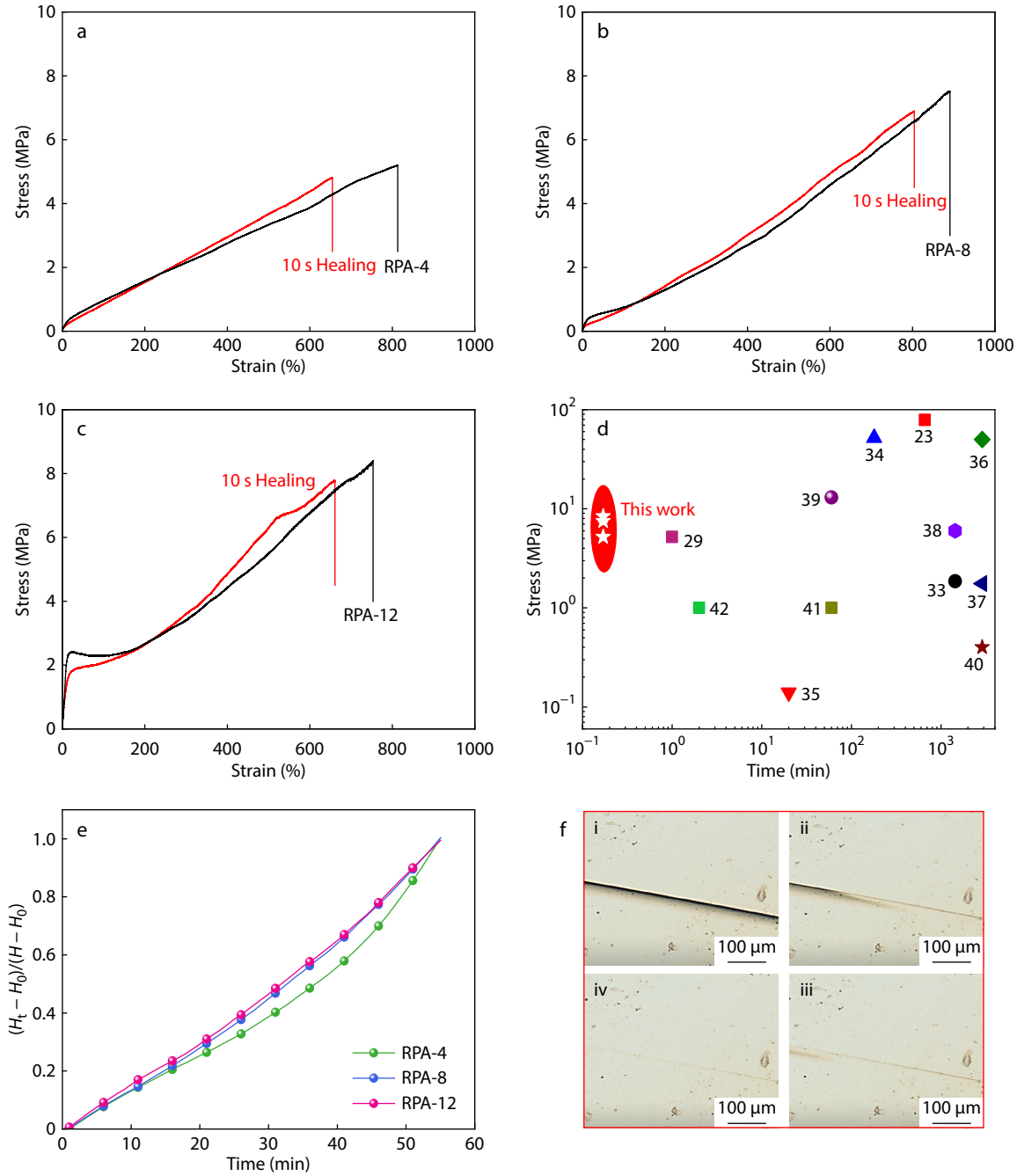

Fig. 3 Stress-strain curves of virgin (black) and healed (red) samples of RPA-4 (a), RPA-8 (b) and RPA-12 (c); (d) The healing time needed for the resultant polymers and recently reported room-temperature self-healing polymers with separated phase domain; (e) The normalized peak height of C=O group with time in the sequential scanning spectra calculated from Fig. S8 (in ESI); (f) The optical micrographs taken during the healing process of RPA-4 at time periods of (i) 0 s, (ii) 10 s, (iii) 20 s, (iv) 30 s.

https://doi.org/10.1007/s10118-024-3097-5

than previously reported self-healing elastomers with separated phase domain, as shown in Fig. 3(d).[23,32–42]

It is well known that the large amount of dissociated hydrogen bonds at the fracture surfaces, which can re-bond once they encounter, are responsible for the fast self-healing ability.[43,44] Based on this, we infer that the decrease of MSPD can facilitate the re-bonding of hydrogen bonds, which improves the healing efficiency of the polymers, even if the migration of polymer chains is restricted. To verify this deduction, the re-bonding process of the hydrogen bonds of RPA-n were followed *in situ* by Fourier transform infrared (FTIR) spectroscopy as below, the sample was first heated to 130 °C to dissociate the hydrogen bonds and the re-bonding process of it during cooling (with a cooling rate of 2 °C) was followed by FTIR measurements. For clarity, the time dependent difference FTIR spectra of RPA-*n* are shown in Figs. S8(a)–S8(c) (in ESI). From Figs. S8(a)–S8(c) (in ESI), it is obvious that the intensities of the hydrogen bonded C=O at 1633 cm^{-1} in RPA-*n* increase with the decrease of temperature. On the other hand, the peak intensities of the free C=O at 1651 cm^{-1} display an inverse tendency with the hydrogen bonded C=O, indicating a gradual re-bonding of hydrogen bonds upon cooling. To further disclose the re-bonding rate of the hydrogen bonds, Fig. 3(e) shows the plots of normalized peak height of hydrogen bonded C=O versus time for RPA-*n*. From Fig. 3(e), it is clear that the peak height of hydrogen bonded C=O in RPA-12 exhibits the highest variation rate at the used condition, whereas that in RPA-4 displays the lowest changing rate. The times needed for re-bonding of *ca.* 50% hydrogen bonds are estimated to be 37, 32 and 31 min for RAP-4, 8 and 12, respectively. Therefore, RPA-12 exhibits the highest healing efficiency after healing for 10 s. In addition, RPA-*n* exhibits excellent scratch healing capability. As shown in Fig. 3(f), the artificial scratch on RPA-4 surface disappears completely after *ca.* 30 s at room temperature (see Figs. 3f-i–3f-iv and Video S1 in ESI), demonstrating the excellent self-healing performance of it.

CONCLUSIONS

In summary, we established an intelligent method to fabricate self-healing polymers with tunable phase structure without changing the proportion of monomers. The chains of the resultant polymer contain two segments, *i.e.*, random P(ACMO-*co*-MPEG) and PACMO segments. The hydrophobic interactions among PACMO segments compel them together to form separated phase structures with the size of separated phase domain to be simply regulated by tuning the molecular weight of PACMO segment. It was found that the phase separation structure can definitely improve the mechanical strength of polymers, which increases with decrease of phase domain size. Most importantly, the decrease of phase size can facilitate the re-bonding rate of hydrogen bonds and thus enhance the self-healing efficiency of the polymers significantly.

Conflict of Interests

The authors declare no interest conflict.

Electronic Supplementary Information

Electronic supplementary information (ESI) is available free of charge in the online version of this article at http://doi.org/10.1007/s10118-024-3097-5.

Data Availability Statement

The associated data of this article (DOI: 10.1007/s10118-024-3097-5) can be accessed from the *Chinese Journal of Polymer Science* database (https://www.cjps.org).

ACKNOWLEDGMENTS

This work was financially supported by the Natural Science Foundation of Shandong Province (No. ZR2022MB122), "Qingchuang science and technology plan" project of colleges and Universities in Shandong Province (No. 2020KJC005).

REFERENCES

1 Sumerlin, B. S. Next-generation self-healing materials. *Science* **2018**, *362*, 150–151.
2 Zhang, M. Self-healing polymeric materials: on a winding road to success. *Chinese J. Polym. Sci.* **2022**, *40*, 1315–1316.
3 Xu, J.; Zhu, L.; Nie, Y.; Li, Y.; Wei, S.; Chen, X.; Zhao, W.; Yan, S. Advances and challenges of self-healing elastomers: a mini review. *Materials* **2022**, *15*, 5993.
4 Zheng, Y.; Zhu, H.; Tan, Y.; Liu, F.; Wu, Y. Rapid self-healing and strong adhesive elastomer *via* supramolecular aggregates from core-shell micelles of silicon hydroxyl-functionalized *cis*-polybutadiene. *Chinese J. Polym. Sci.* **2023**, *41*, 84–94.
5 Guo, Z.; Lu, X.; Wang, X.; Li, X.; Li, J.; Sun, J. Engineering of chain rigidity and hydrogen bond cross-linking toward ultra-strong, healable, recyclable and water-resistant elastomers. *Adv. Mater.* **2023**, *35*, 2300286.
6 Li, C.; Liu, J.; Qiu, X.; Yang, X.; Huang, X.; Zhang, X. Photoswitchable and reversible fluorescent eutectogels for conformal information encryption. *Angew. Chem. Int. Ed.* **2023**, *62*, 13971.
7 Wang, Y.; Shu, R.; Zhang, X. Strong, supertough and self-healing biomimetic layered nanocomposites enabled by reversible interfacial polymer chain sliding. *Angew. Chem. Int. Ed.* **2023**, *62*, 03446.
8 Yang, T.; Lu, X.; Wang, X.; Li, Y.; Wei, X.; Wang, W.; Sun, J. Healable, recyclable, and scratch-resistant polyurethane elastomers cross-linked with multiple hydrogen bonds. *ACS Appl. Polym. Mater.* **2023**, *5*, 2830–2839.
9 Zhao, C.; Guo, M.; Mao, J.; Li, Y.; Wu, Y.; Guo, H.; Xiang, D.; Li, H. Self-healing, stretchable, temperature-sensitive and strain-sensitive hydrogel-based flexible sensors. *Chinese J. Polym. Sci.* **2023**, *41*, 334–344.
10 Zhang, L.; You, Z. Dynamic oxime-urethane bonds, a versatile unit of high performance self-healing polymers for diverse applications. *Chinese J. Polym. Sci.* **2021**, *39*, 1281–1291.
11 Neal, J. A.; Mozhdehi, D.; Guan, Z. Enhancing mechanical performance of a covalent self-healing material by sacrificial non-covalent bonds. *J. Am. Chem. Soc.* **2015**, *137*, 4846–4850.
12 Chen, Y.; Guan, Z. Multivalent hydrogen bonding block copolymers self-assemble into strong and tough self-healing materials. *Chem. Commun.* **2014**, *50*, 10868–10870.
13 Li, M.; Rong, M.; Zhang, M. Reversible mechanochemistry enabled

autonomous sustaining of robustness of polymers—an example of next generation self-healing strategy. *Chinese J. Polym. Sci.* **2021**, *39*, 545–553.
14 Eom, Y.; Kim, S.-M.; Lee, M.; Jeon, H.; Park, J.; Lee, E. S.; Hwang, S. Y.; Park, J.; Oh, D. X. Mechano-responsive hydrogen-bonding array of thermoplastic polyurethane elastomer captures both strength and self-healing. *Nat. Commun.* **2021**, *12*, 621.
15 Wang, Y.; Huang, X.; Zhang, X. Mechano-responsive hydrogen-bonding array of thermoplastic polyurethane elastomer captures both strength and self-healing. *Nat. Commun.* **2021**, *12*, 1291.
16 Sun, F.; Liu, L.; Liu, T.; Wang, X.; Qi, Q.; Hang, Z.; Chen, K.; Xu, J.; Fu, J. Vascular smooth muscle-inspired architecture enables soft yet tough self-healing materials for durable capacitive strain-sensor. *Nat. Commun.* **2023**, *14*, 130.
17 Tie, J.; Mao, Z.; Zhang, L.; Zhong, Y.; Xu, H. Strong and ultratough ionogel enabled by ingenious combined ionic liquids induced microphase separation. *Adv. Funct. Mater.* **2023**, 2307367.
18 Li, H.; Li, X.; Liu, N.; Liu, D.; Wang, Z.; Chen, F. A tough and strain-stiffening ionogel enabled by moderate microphase separation for epidermal multi-sensor. *Polymer* **2023**, *282*, 126166.
19 Wu, J.; Zhang, Z.; Wu, Z.; Liu, D.; Yang, X.; Wang, Y.; Jia, X.; Xu, X.; Jiang, P.; Wang, X. A tough and strain-stiffening ionogel enabled by moderate microphase separation for epidermal multi-sensor. *Adv. Funct. Mater.* **2022**, *33*, 2210395.
20 Liu, Y.; Chen, L.; Yang, Y.; Chen, H.; Zhang, X.; Liu, S. High Mechanical Strength and Multifunctional Microphase-Separated Supramolecular Hydrogels Fabricated by Liquid-Crystalline Block copolymer. *Macromol. Rapid Commun.* **2022**, *44*, 2200829.
21 Lai, Y.; Kuang, X.; Zhu, P.; Huang, M.; Dong, X.; Wang, D. Colorless, transparent, robust, and fast scratch-self-healing elastomers *via* a phase-locked dynamic bonds design. *Adv. Mater.* **2018**, *30*, 1802556.
22 Wang, B.; Zhai, W.; Fan, J. B.; Xu, J.; Zhao, W.; Feng, X. An interfacially polymerized self-healing organo/hydro copolymer with shape memory. *Nanoscale* **2019**, *11*, 6846–6851.
23 An, N.; Wang, X.; Li, Y.; Zhang, L.; Lu, Z.; Sun, J. Healable and mechanically super-strong polymeric composites derived from hydrogen-bonded polymeric complexes. *Adv. Mater.* **2019**, *31*, 1904882.
24 Xun, X.; Zhao, X.; Li, Q.; Zhao, B.; Ouyang, T.; Zhang, Z.; Kang, Z.; Liao, Q.; Zhang, Y. Tough and degradable self-healing elastomer from synergistic soft-hard segments design for biomechano-robust artificial skin. *ACS Nano* **2021**, *15*, 20656–20665.
25 Xie, Z.; Hu, B.; Li, R.; Zhang, Q. Hydrogen bonding in self-healing elastomers. *ACS Omega* **2021**, *6*, 9319–9333.
26 Zhao, W.; Liu, Y.; Zhao, C.; Shi, X.; Feng, X.; Xu, J.; Wang, S.; Wu, Y.; Yan, S. A fast self-healable and stretchable conductor based on hierarchical wrinkled structure for flexible electronics. *Compos. Sci. Technol.* **2021**, *211*, 108834.
27 Zhao, W.; Zhang, Z.; Hu, J.; Feng, X.; Xu, J.; Wu, Y.; Yan, S. Robust and ultra-fast self-healing elastomers with hierarchically anisotropic structures and used for wearable sensors. *Chem. Eng. J.* **2022**, *446*, 137305.
28 Zhao, W.; Li, Y.; Hu, J.; Feng, X.; Zhang, H.; Xu, J.; Yan, S. Mechanically robust, instant self-healing polymers towards elastic entropy driven artificial muscles. *Chem. Eng. J.* **2023**, *454*, 140100.
29 Zhao, W.; Liu, Y.; Zhang, Z.; Feng, X.; Xu, H.; Xu, J.; Hu, J.; Wang, S.; Wu, Y.; Yan, S. High-strength, fast self-healing, aging-insensitive elastomers with shape memory effect. *ACS Appl. Mater. Interfaces* **2020**, *12*, 35445–35452.
30 Li, Y.; Feng, X.; Sui, C.; Xu, J.; Zhao, W.; Yan, S. Highly entangled elastomer with ultra-fast self-healing capability and high mechanical strength. *Chem. Eng. J.* **2024**, *479*, 147689.
31 Lai, J.; Filla, D.; Shea, R. Functional polymers from novel carboxyl-terminated trithiocarbonates as highly efficient RAFT agents. *Macromolecules* **2002**, *35*, 6754–6756.
32 Pan, J.; Zeng, H.; Gao, L.; Zhang, Q.; Luo, H.; Shi, X.; Zhang, H. Hierarchical multiscale hydrogels with identical compositions yet disparate properties *via* tunable phase separation. *Adv. Funct. Mater.* **2022**, *32*, 2110277.
33 Chen, Y.; Kushner, A.; Williams, G.; Guan, Z. Multiphase design of autonomic self-healing thermoplastic elastomers. *Nat. Chem.* **2012**, *4*, 467–472.
34 Wang, X.; Zhan, S.; Lu, Z.; Li, J.; Yang, X.; Qiao, Y.; Men, Y.; Sun, J. Healable, recyclable, and mechanically tough polyurethane elastomers with exceptional damage tolerance. *Adv. Mater.* **2020**, *32*, 2005759.
35 Xiang, H.; Li, X.; Wu, B.; Sun, S.; Wu, P. Highly damping and self-healable ionic elastomer from dynamic phase separation of sticky fluorinated polymers. *Adv. Mater.* **2023**, *35*, 2209581.
36 Yao, Y.; Liu, B.; Xu, Z.; Yang, J.; Liu, W. An unparalleled H-bonding and ion-bonding crosslinked waterborne polyurethane with super toughness and unprecedented fracture energy. *Mater. Horiz.* **2021**, *8*, 2742.
37 Zhang, Q.; Niu, S.; Wang, L.; Lopez, J.; Chen, S.; Cai, Y.; Du, R.; Liu, Y.; Lai, J.; Liu, L.; Li, C.; Yan, X.; Liu, C.; Tok, J.; Jia, X.; Bao, Z. An elastic autonomous self-healing capacitive sensor based on a dynamic dual crosslinked chemical system. *Adv. Mater.* **2018**, *30*, 1801435.
38 Peng, Y.; Zhao, L.; Yang, C.; Yang, Y.; Song, C.; Wu, Q.; Huang, G.; Wu, J. Super tough and strong self-healing elastomers based on polyampholytes. *J. Mater. Chem. A* **2018**, *6*, 19066.
39 Zhao, P.; Yin, C.; Zhang, Y.; Chen, X.; Yang, B.; Xia, J.; Bian, L. Mussel cuticle-mimetic ultra-tough, self-healing elastomers with double-locked nanodomains exhibit fast stimuli-responsive shape transformation. *J. Mater. Chem. A* **2020**, *8*, 12463.
40 Su, G.; Yin, S.; Guo, Y.; Zhao, F.; Guo, Q.; Zhang, X.; Zhou, T.; Yu, G. Balancing the mechanical, electronic, and self-healing properties in conductive self-healing hydrogel for wearable sensor applications. *Mater. Horiz.* **2021**, *8*, 1795.
41 Yang, Y.; Wang, H.; Huang, L.; Nishiura, M.; Higaki, Y.; Hou, Z. Terpolymerization of ethylene and two different methoxyaryl-substituted propylenes by scandium catalyst makes tough and fast self-healing elastomers. *Angew. Chem. Int. Ed.* **2021**, *60*, 26192–26198.
42 Tang, M.; Li, Z.; Wang, K.; Jiang, Y.; Tian, M.; Qin, Y.; Gong, Y.; Li, Z.; Wu, L. Ultrafast self-healing and self-adhesive polysiloxane towards reconfigurable on-skin electronics. *J. Mater. Chem. A* **2022**, *10*, 1750–1759.
43 Xu, J.; Chen, J.; Zhang, Y.; Liu, T.; Fu, J. A fast room-temperature self-healing glassy polyurethane. *Angew. Chem. Int. Ed.* **2021**, *60*, 7947–7955.
44 Tee, B. C. K.; Wang, C.; Allen, R.; Bao, Z. A fast room-temperature self-healing glassy polyurethane. *Nat. Nanotechnol.* **2012**, *7*, 825–832.

https://doi.org/10.1007/s10118-024-3097-5